Tangling of Tethered Swimmers: Interactions between Two Nematodes

Matilda Backholm,[1] Rafael D. Schulman,[1] William S. Ryu,[2] and Kari Dalnoki-Veress[1,3,*]
[1]Department of Physics & Astronomy and the Brockhouse Institute for Materials Research, McMaster University, Hamilton, Ontario L8S 4M1, Canada
[2]Department of Physics and the Donnelly Centre, University of Toronto, Toronto, Ontario M5S 1A7, Canada
[3]Laboratoire de Physico-Chimie Théorique, UMR CNRS Gulliver 7083, ESPCI, Paris, France
(Received 9 June 2014; published 23 September 2014)

The tangling of two tethered microswimming worms serving as the ends of "active strings" is investigated experimentally and modeled analytically. *C. elegans* nematodes of similar size are caught by their tails using micropipettes and left to swim and interact at different separations over long times. The worms are found to tangle in a reproducible and statistically predictable manner, which is modeled based on the relative motion of the worm heads. Our results provide insight into the intricate tangling interactions present in active biological systems.

DOI: 10.1103/PhysRevLett.113.138101 PACS numbers: 87.85.gj, 46.70.Hg, 47.63.Gd

Entanglements are ubiquitous in our everyday lives with headphone cords forming braids and knots in our pockets, collections of small items like staples arranging into large tangled networks [1], and hair strands knotting into disordered snarls [2]. A less common example is the knotting of the umbilical cord which occurs at birth for about 1% of the population [3]. At smaller scales, like in the case of DNA, knots occur naturally in the recombination and replication cycles and are thought to contribute to gene regulation [4–6]. Tangling in polymers [7], proteins [3], and the flagella in groups of spermatozoa [8,9] as well as bacteria are further examples. Flagellar entanglements have been shown to stabilize bacterial networks in biofilms [10,11] and also give rise to the well-studied run-and-tumble motion of bacteria, where several flagella are tangled into a propellerlike bundle, allowing for propulsion in a specific direction [12–14].

Over recent years, active networks of, e.g., highly packed bacteria [15,16], cilia [17–20], nematodes [21,22], sperm cells [23], self-locomoting slender rods [24], microtubule filaments [25,26], and colloidal particles [27] have been studied for the purpose of bioengineering applications [28] and understanding the complex, collective interactions present in these living or active liquids [29,30]. In addition to hydrodynamic coupling and collisions, entanglements play a vital role in determining the final physical properties and biological function of the active material. In the case of cilia, for example, the synchronized beating enables locomotion of a variety of microorganisms as well as the transport of mucus from our lungs. Any tangling of the cilium strands would certainly have severe biological consequences.

Mathematicians and physicists have taken a keen interest in understanding the formation and topology of knots and tangles. To spontaneously form a knot, a long and flexible string with a certain excluded volume and bending stiffness has to be given enough energy to move around and explore its surroundings [31]. For very small strings, like polymer chains, thermal energy is sufficient to reptate and entangle the molecules [7]. For larger objects, however, extra energy input is needed, as in the case of the driven helical rotation of bacterial flagella [12–14] or for vigorously shaken ball chains and strings [32–35]. Independent of the formation strategy, the tangle topology can be defined by the Conway notation [36–40].

The formation, lifetime, and untying of knots has been investigated experimentally in macroscopic systems consisting of single strings, chains, and ropes of different lengths and stiffnesses [32–35]. Upon shaking these passive strings, self-induced knots of different types were found, and the knotting probability was theoretically modeled. Most knots form and disappear due to the string ends moving in and out of chain loops and around straight segments of the chain. To the best of our knowledge, this intricate chain end motion has not been closely studied, nor has the interaction between two chain ends.

Here we present a time-resolved experimental system illustrated in Fig. 1(a), probing the dynamic tangling of two

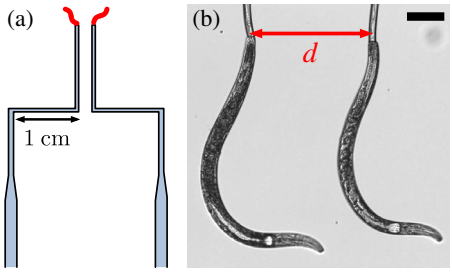

FIG. 1 (color online). (a) Schematic illustration of the experimental setup where two worms were held by *Z*-shaped micropipettes. (b) Optical microscopy image of two young adult *C. elegans* worms swimming at a separation d. Scale bar 200 μm.

small worms serving as active, i.e., self-driven, strings on a millimetric scale. The nematode *Caenorhabditis elegans* is a millimeter-sized microswimmer used as a model organism to probe undulatory locomotion experimentally [41–45]. When tail anchored, *C. elegans* has been shown to move in a highly reproducible, undulatory fashion with a well-defined frequency and amplitude [43]. In our experiments, the nematodes were placed in a buffer solution and held by their tails with long (~2 cm) and thin (~20 μm) micropipettes made as described in Refs. [46,47], and carefully placed side by side at a separation d as shown in Fig. 1(b) (see the Supplemental Material for more experimental details [48]). The motion of the worms was monitored with a camera (56 fps) as shown in the time-lapse snapshots of Fig. 2(a) (see the Supplemental Material movie SM1.avi [48]). The lateral positions of the worm heads were tracked and are plotted as a function of time in Fig. 2(b), where sinusoidal functions have been fit to the three first noninteracting periods of both worms, showing the smooth, undulatory motion of the swimmers.

At close enough distances, the worms were seen to frequently overlap and form temporary tangles. A typical example of the formation of such a tangle is shown by the head positions in Fig. 2(b). The undulatory motion of the slender bodies remains unchanged throughout a tangle, deeming the attempt frequency to untangle the same as the swimming frequency of the worms, which finally exit the locked configuration by moving their heads apart. The undoing of the tangle is sometimes driven by the motion of only one of the worms.

Here, two different types of tangles shown in Figs. 2(c) and 2(d) were found to occur frequently and in a reproducible manner. These could be recognized by the number of overlapping points and are here defined as a 2- and 3-tangle, respectively (in the Conway notation, these tangles would correspond to vertical rational tangles of type $1/2$ and $1/3$ [36]). To understand the formation of these specific tangles, the worms were modeled as strings with an average length $L \sim L_{\text{left}} \sim L_{\text{right}}$ and radius R. Consistent with our observations, the lateral position of the string ends (worm heads) were defined as sinusoidal functions with a maximum amplitude of $A = kL$, where k is an experimentally determinable constant. The left and right string end positions could, thus, be written as $x_L = A\sin(t+\phi)$ and $x_R = A\sin t + d$, respectively, where $\phi \in [0,\pi]$ is the phase shift between the active strings, and $d > 0$ is the distance between their anchors.

The probability of these strings entangling will vanish at large distances and become increasingly probable as the string ends start to overlap, i.e., at some point in time, $x_L \geq x_R$. This results in a critical ratio between the distance and amplitude for any overlap to be possible: $d/A \leq \sin(t+\phi) - \sin t$. For an entanglement to be physically possible, it is not sufficient for only the string ends to overlap. Instead, a certain fraction (L_c/L) of each string needs to be available to form a full tangle with a minimum length of L_c. We, therefore, consider that both worms must have a swimming amplitude such that they reach a distance greater than L_c beyond the symmetry plane [exemplified by the left worm in the second frame of Fig. 2(a)]. Thus, we

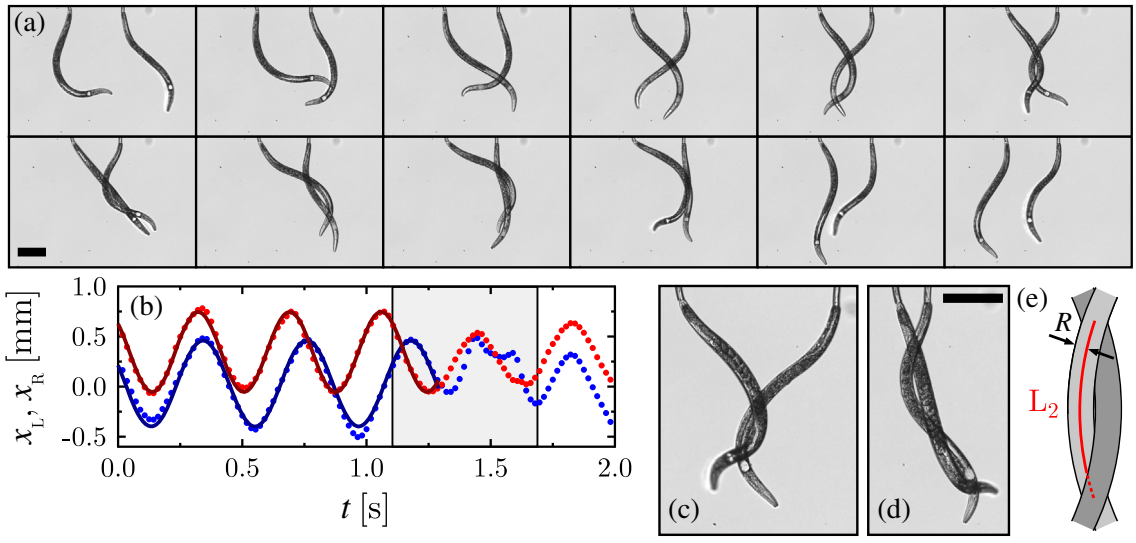

FIG. 2 (color online). (a) Snapshots (0.054 s between each image) showing the tangling of two worms swimming at a distance $d = 370$ μm apart. (b) The lateral position of the heads of the same worms. The worms slowly shift from in-phase to out-of-phase swimming, allowing the heads to overlap and the worms to wrap around each other's bodies and form a tangle. Subsequently, they exit the tangle in phase with the same sinusoidal motion as prior to the tangling event. The gray zone in the graph denotes the time frame of the snapshots in (a) (image of every third data point shown). The solid lines are sinusoidal fits to the head positions of both of the worms. (c),(d) Two worms at different separations forming a 2- and 3-tangle, respectively. (e) A schematic illustration of a 2 tangle modeled as a helix with radius R, twist π, and arc length L_2. All scale bars represent 200 μm.

can state that for a tangle to occur, $A \geq d/2 + L_c$, which yields

$$\frac{L}{d} \geq \left[2\left(k - \frac{L_c}{L}\right)\right]^{-1}. \quad (1)$$

This equation corresponds to an upper bound to the critical ratio between the chain length and distance for an entanglement to be theoretically possible.

The lowest-order tangle seen in our system is the 2 rational tangle [Fig. 2(c)] illustrated schematically in Fig. 2(e). This tangle can be described as a helix with a radius R (the same as the worm radius), curvature κ, and twist π. The arc length (minimum string length required for this tangle) then is $L_c = L_2 = \pi\sqrt{R/\kappa}$. The proportionality constant relating the maximum swimming amplitude (see the Supplemental Material [48]) to the worm length has been measured as $k = 0.8 \pm 0.05$ for single worms. By measuring the mean radius and length of the worms used in this study (young adults and adults, $R = 29 \pm 2$ μm and $L = 1080 \pm 70$ μm) and the mean of the absolute curvature of the first (anterior) half of their bodies in a state of normal swimming ($\kappa = 3.3 \pm 0.2$ mm^{-1}), an estimate of $L_2/L = 0.27 \pm 0.02$ could, thus, be made. By applying the helix model to Eq. (1), the predicted critical ratio between the worm length and distance for any entanglement to be possible is $(L/d)_2 \geq 0.95 \pm 0.10$. Following the same approach, the critical ratio for a 3 tangle modeled as a helix with a twist of 2π is calculated as $(L/d)_3 = 2.0 \pm 0.3$.

The experiments were performed at different distances with several pairs of worms of similar size. In a particular experiment, the presence of 2- and 3-tangles were noted. In Fig. 3(a), we plot if a tangle could be observed at a given ratio L/d and also indicate the type of tangle. The two vertical lines in the graph denote the theoretically predicted critical ratios $(L/d)_2$ and $(L/d)_3$, and the experimental onsets are, within error, in excellent agreement with the model. Note that 2 tangles were always present in experiments in which 3 tangles were observed.

In Figs. 3(b) and 3(c), the distributions of entanglement lifetimes are shown for several experiments performed in the two extreme cases of large ($L/d = 1.0 \pm 0.2$) and small ($L/d = 5.7 \pm 2.8$) separations, respectively (for further details, see the Supplemental Material [48]). At the larger separation, only 2 tangles are possible and have an average lifetime of $\tau_2 = 0.18 \pm 0.03$ s. However, for the shorter separation, both 2- and 3-tangles were possible, and this is clearly seen in Fig. 3(c) where a shoulder around $\tau_3 \approx 0.4$ s $\approx 2\tau_2$ has formed due to the occurrence of the more long-lived 3 tangle stabilized by an additional crossing which requires extra time to become undone. Note that, as one might expect, even for short distances, the 3 tangles are much less probable than 2 tangles. A slight shift and widening of the 2 peak at close distances is also apparent

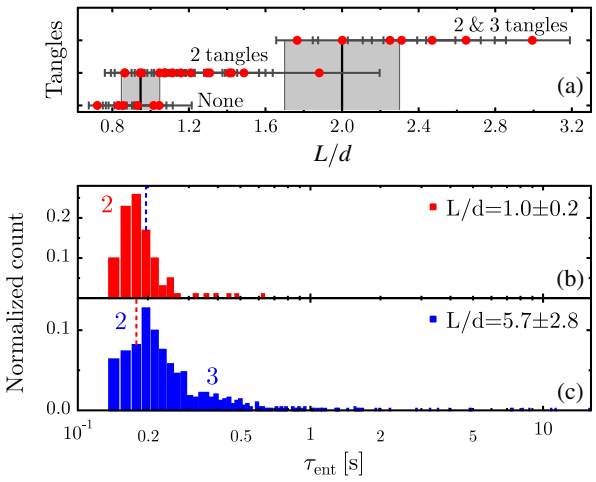

FIG. 3 (color online). (a) The experimental onset of 2- and 3-tangles (filled circles) with horizontal error bars as a function of the worm length-distance ratio. The vertical lines are the theoretical crossover predictions $(L/d)_2 = 0.95 \pm 0.10$ and $(L/d)_3 = 2.0 \pm 0.3$. (b),(c) Histograms of the entanglement lifetimes of several worm pairs far apart [$L/d = 1.0 \pm 0.2$, (b)] and close together [$L/d = 5.7 \pm 2.8$, (c)]. The count has been normalized with the total number of tangles. The vertical dashed lines indicate the peak position of the other histogram.

when comparing the two distributions [see vertical dashed lines in Figs. 3(b) and 3(c)], indicating more variations in the tangling events as the worms are brought closer together. A few 3 tangles remained stable for around 10 s, which corresponds to over 20 full swimming cycles (untangling attempts). These dynamic tangles were beating and rotating reminiscent of bacterial bundles (see the Supplemental Material movie SM2.avi [48]). Variables that affect the tangle stability are the length, thickness, and bending stiffness of the worms, the attempt frequency to untangle, the friction between the worms [49], as well as contact between the worms eliciting mechanosensory responses [50]. The latter of these has previously been shown not to affect the collective swimming of *C. elegans* [21] and did not seem to strongly affect the tangling dynamics in our experiments either.

To investigate the entanglement probability as L/d increases above the critical ratios derived above, we now follow the lateral motion of the point (x_c) on the worm body located at a distance of L_c from the head. Since the worm propagates traveling waves down its body, $x_c(t)$ can also be modeled as a sinusoidal function with an amplitude $A_c = k_c L$, where k_c is an experimentally determinable constant. For the left and right worms, we thereby have $x_{c,L} = A_c \sin(t + \phi)$ and $x_{c,R} = A_c \sin t + d$, respectively. At a given separation distance, these sinusoidal functions intersect at a range of phase shifts above some critical value. For an entanglement to be possible, the maximum value of the difference $\Delta = x_{c,L} - x_{c,R}$ needs to be greater than zero. Using a trigonometric

identity, $x_{c,L} - x_{c,R} = 2A_c \cos[(2t+\phi)/2]\sin(\phi/2) - d$. Maximizing this difference with respect to time yields $\Delta = 2A_c \sin(\phi/2) - d \geq 0$ and, thus,

$$\phi \geq \phi_c = 2\sin^{-1}\left(\frac{d}{2A_c}\right). \quad (2)$$

This is the critical phase shift needed to form a tangle at a specific L/d ratio. In other words, the farther apart the worms are, the more out of phase they have to swim in order to intersect and the smaller is the range of phase shifts which yield intersections.

Although the worms have very similar average frequencies ($f = 2.1 \pm 0.2$ Hz), small temporal variations in this quantity allow the worms to explore all relative phase shifts, as exemplified in Fig. 2(b). Since the worms explore all relative phase shifts over time, and since a certain fraction of intersection events between the worm ends will lead to entanglements, it is reasonable to hypothesize that the entanglement probability will be proportional to the fraction of relative phase shifts which contain an intersection at the separation distance d. However, we also expect that entanglement events will be more likely to occur if the worm heads have more space (and time) to wrap around each other's bodies. Thus, we make the first-order assumption that the probability of entanglements at a given separation distance is proportional to the fraction of relative phase shifts which contain an intersection but where each phase shift is linearly weighted by the maximum separation between the worm heads, giving

$$p \propto \int_{\phi_c}^{\pi} \frac{\Delta}{L} d\phi, \quad (3)$$

where L is used to nondimensionalize the weighting. Evaluating this integral and substituting $A_c = k_c L$ gives

$$p \propto 2k_c\sqrt{4 - \left(\frac{d}{k_c L}\right)^2} - \frac{d}{L}\left[\pi - 2\sin^{-1}\left(\frac{d}{2k_c L}\right)\right], \quad (4)$$

which shows how the entanglement probability scales with the worm length-distance ratio.

The number of worm entanglements were counted, and the experimental entanglement probability was calculated as the ratio between the number of entanglements and entanglement attempts (the sum of the number of swimming cycles and successful tangling events). The probability is plotted as a function of L/d in Fig. 4 for all experiments performed with different worm pairs at different distances. The entanglement probability increases sharply at a worm separation close to one worm length. Equation (4) is successfully fit to the data, and the model is clearly in excellent agreement with the experimental observations. Two fitting parameters were used to fit the data in Fig. 4. The first is a compressing factor (0.11 ± 0.03) in the y direction, which corresponds to the proportionality prefactor of Eq. (4). Any mechanosensory interactions present between the worms would enter into this factor. The second fitting parameter defines the horizontal shift of the theoretical curve and is given by $k_c = 0.64 \pm 0.10$. Comparing this value to that derivable from the helix model giving $A_{c,\mathrm{helix}}/L = k - L_2/L = 0.53 \pm 0.05$, we find the two models to be, within error, in excellent agreement.

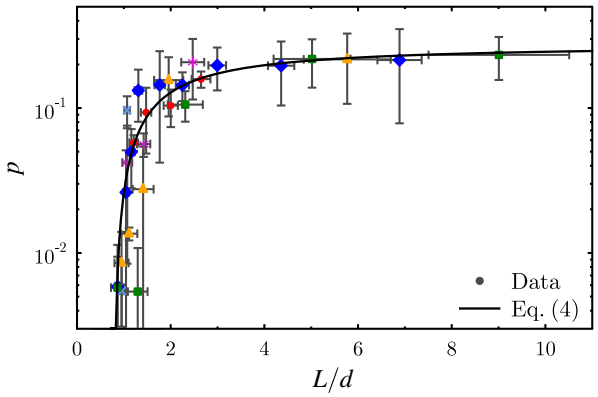

FIG. 4 (color online). The entanglement probability as a function of L/d. The different markers denote experiments with different worm pairs. The solid line is the analytical fit of Eq. (4) to the data.

To form a tangle in our experiments, the worms were forced to deviate from their otherwise planar swimming motion to form a three-dimensional helix. If significant out-of-plane swimming occurred, the entanglement probability was seen to vastly decrease, as easily explained by our geometric model. The clear entanglement difference between the nearly 2D versus a complete 3D motion could, thus, be a significant factor in, e.g., how arrays of cilia avoid tangling due to their sophisticated 3D motion [51]. The aspect ratio of cilia can be as high as $L/D = 100$ (versus 19 for our worms), where D is the diameter. Since cilia are typically arranged at distances 0.27–0.4 μm apart [52], $(L/d)_{\mathrm{cilia}} = 75$. The lack of ciliar entanglements is, thus, surprising when compared to our experimental findings in planar swimming and highlights the importance of the specific motion patterns used to avoid or achieve a tangled network. Strong hydrodynamic interactions could also act to modify ciliar entanglements at close distances. Hydrodynamic interactions were not discovered between the worms in our experiments, consistent with the findings of others [21].

Here we have presented a time-resolved, dynamic study of the tangling of active stringlike worms. By describing the system with a simple model based on the overlap probability of the worm heads during their undulatory swimming, the critical ratio between the worm length and distance for any entanglement to be possible was

quantitatively predicted and shown to be in excellent agreement with experimental observations. Furthermore, the entanglement probability was analytically derived and successfully fit to the data. It is clear that the tangling of the active strings is far from random but a statistically predictable process based on the relative motion of their ends. These experiments provide an interesting model system to understand the intricate interactions present in active matter such as cilia and bacterial flagella.

The financial support by NSERC of Canada is gratefully acknowledged. The authors also thank Solomon Barkley for helpful discussions.

*dalnoki@mcmaster.ca

[1] N. Gravish, S. V. Franklin, D. L. Hu, and D. I. Goldman, Phys. Rev. Lett. **108**, 208001 (2012).
[2] D. T. English and H. E. Jones, Arch. Dermatol. **107**, 77 (1973).
[3] A. Goriely, in *Physical and Numerical Models in Knot Theory*, edited by J. A. Calvo, K. C. Millett, E. J. Rawdon, and A. Stasiak (World Scientific, Singapore, 2005), Chap. 6.
[4] S. A. Wasserman and N. R. Cozzarelli, Science **232**, 951 (1986).
[5] E. Ercolini, F. Valle, J. Adamcik, G. Witz, R. Metzler, P. De Los Rios, J. Roca, and G. Dietler, Phys. Rev. Lett. **98**, 058102 (2007).
[6] J. Tang, N. Du, and P. S. Doyle, Proc. Natl. Acad. Sci. U.S.A. **108**, 16153 (2011).
[7] P.-G. de Gennes, Macromolecules **17**, 703 (1984).
[8] K. J. Eckelbarger, C. M. Young, and J. L. Cameron, Biol. Bull. **176**, 257 (1989).
[9] D. M. Woolley and G. G. Vernon, J. Exp. Biol. **204**, 1333 (2001).
[10] C. J. Ingham and E. Ben-Jacob, BMC Microbiol. **8**, 36 (2008).
[11] D. O. Serra, A. M. Richter, G. Klauck, F. Mika, and R. Hengge, mBio **4**, e00103-13 (2013).
[12] L. Turner, W. S. Ryu, and H. C. Berg, J. Bacteriol. **182**, 2793 (2000).
[13] R. M. Macnab, Proc. Natl. Acad. Sci. U.S.A. **74**, 221 (1977).
[14] M. Kim, J. C. Bird, A. J. Van Parys, K. S. Breuer, and T. R. Powers, Proc. Natl. Acad. Sci. U.S.A. **100**, 15481 (2003).
[15] M. F. Copeland and D. B. Weibel, Soft Matter **5**, 1174 (2009).
[16] J. Dunkel, S. Heidenreich, K. Drescher, H. H. Wensink, M. Bär, and R. E. Goldstein, Phys. Rev. Lett. **110**, 228102 (2013).
[17] L. Gheber and Z. Priel, Biophys. J. **55**, 183 (1989).
[18] S. Gueron, K. Levit-Gurevich, N. Liron, and J. J. Blum, Proc. Natl. Acad. Sci. U.S.A. **94**, 6001 (1997).
[19] P. Lenz and A. Ryskin, Phys. Biol. **3**, 285 (2006).
[20] S. Michelin and E. Lauga, Phys. Fluids **22**, 111901 (2010).
[21] J. Yuan, D. M. Raizen, and H. H. Bau, Proc. Natl. Acad. Sci. U.S.A. **111**, 6865 (2014).
[22] S. Gart, D. Vella, and S. Jung, Soft Matter **7**, 2444 (2011).
[23] H. S. Fisher, L. Giomi, H. E. Hoekstra, and L. Mahadevan, Proc. R. Soc. B **281**, 20140296 (2014).
[24] D. Saintillan and M. J. Shelley, Phys. Rev. Lett. **99**, 058102 (2007).
[25] T. Sanchez, D. Welch, D. Nicastro, and Z. Dogic, Science **333**, 456 (2011).
[26] T. Sanchez, D. T. N. Chen, S. J. DeCamp, M. Heymann, and Z. Dogic, Nature (London) **491**, 431 (2012).
[27] A. Bricard, J.-B. Caussin, N. Desreumaux, O. Dauchot, and D. Bartolo, Nature (London) **503**, 95 (2013).
[28] N. Darnton, L. Turner, K. Breuer, and H. Berg, Biophys. J. **86**, 1863 (2004).
[29] D. L. Koch and G. Subramanian, Annu. Rev. Fluid Mech. **43**, 637 (2011).
[30] T. Vicsek and A. Zafeiris, Phys. Rep. **517**, 71 (2012).
[31] A. Belmonte, Proc. Natl. Acad. Sci. U.S.A. **104**, 17243 (2007).
[32] A. Belmonte, M. J. Shelley, S. T. Eldakar, and C. H. Wiggins, Phys. Rev. Lett. **87**, 114301 (2001).
[33] E. Ben-Naim, Z. A. Daya, P. Vorobieff, and R. E. Ecke, Phys. Rev. Lett. **86**, 1414 (2001).
[34] J. Hickford, R. Jones, S. Courrech du Pont, and J. Eggers, Phys. Rev. E **74**, 052101 (2006).
[35] D. M. Raymer and D. E. Smith, Proc. Natl. Acad. Sci. U.S.A. **104**, 16432 (2007).
[36] J. H. Conway, in *Computational Problems in Abstract Algebra*, edited by J. Leech (Pergamon Press, New York, 1969), pp. 329–358.
[37] S. A. Bleiler, Trans. Am. Math. Soc. **282**, 385 (1984).
[38] J. R. Goldman and L. H. Kauffman, Adv. Appl. Math. **18**, 300 (1997).
[39] L. H. Kauffman and S. Lambropoulou, Adv. Appl. Math. **33**, 199 (2004).
[40] D. Meluzzi, D. E. Smith, and G. Arya, Annu. Rev. Biophys. **39**, 349 (2010).
[41] S. Brenner, Genetics **77**, 71 (1974).
[42] M. Backholm, W. S. Ryu, and K. Dalnoki-Veress, Proc. Natl. Acad. Sci. U.S.A. **110**, 4528 (2013).
[43] R. D. Schulman, M. Backholm, W. S. Ryu, and K. Dalnoki-Veress, Phys. Rev. E **89**, 050701 (2014).
[44] P. Sauvage, M. Argentina, J. Drappier, T. Senden, J. Siméon, and J.-M. Di Meglio, J. Biomech. **44**, 1117 (2011).
[45] X. N. Shen and P. E. Arratia, Phys. Rev. Lett. **106**, 208101 (2011).
[46] M.-J. Colbert, A. N. Raegen, C. Fradin, and K. Dalnoki-Veress, Eur. Phys. J. E **30**, 117 (2009).
[47] M.-J. Colbert, F. Brochard-Wyart, C. Fradin, and K. Dalnoki-Veress, Biophys. J. **99**, 3555 (2010).
[48] See Supplemental Material http://link.aps.org/supplemental/10.1103/PhysRevLett.113.138101 for experimental details and movies of the worms tangling.
[49] J. H. Maddocks and J. B. Keller, SIAM J. Appl. Math. **47**, 1185 (1987).
[50] R. O'Hagan and M. Chalfie, International review of neurobiology **69**, 169 (2005).
[51] A. Vilfan and F. Jülicher, Phys. Rev. Lett. **96**, 058102 (2006).
[52] Z. Teff, Z. Priel, and L. A. Gheber, Biophys. J. **92**, 1813 (2007).